ELECTROCHEMISTRY

Ultrahigh areal number density solid-state on-chip microsupercapacitors via electrohydrodynamic jet printing

Kwon-Hyung Lee[1], Seong-Sun Lee[1], David B. Ahn[1], Jaehyun Lee[2], Doyoung Byun[2], Sang-Young Lee[1]*

Microsupercapacitors (MSCs) have garnered considerable attention as a promising power source for microelectronics and miniaturized portable/wearable devices. However, their practical application has been hindered by the manufacturing complexity and dimensional limits. Here, we develop a new class of ultrahigh areal number density solid-state MSCs (UHD SS–MSCs) on a chip via electrohydrodynamic (EHD) jet printing. This is, to the best of our knowledge, the first study to exploit EHD jet printing in the MSCs. The activated carbon-based electrode inks are EHD jet-printed, creating interdigitated electrodes with fine feature sizes. Subsequently, a drying-free, ultraviolet-cured solid-state gel electrolyte is introduced to ensure electrochemical isolation between the SS–MSCs, enabling dense SS–MSC integration with on-demand (in-series/in-parallel) cell connection on a chip. The resulting on-chip UHD SS–MSCs exhibit exceptional areal number density [36 unit cells integrated on a chip (area = 8.0 mm × 8.2 mm), 54.9 cells cm^{-2}] and areal operating voltage (65.9 V cm^{-2}).

INTRODUCTION

An ongoing surge in the demand for microelectronics, miniaturized portable/wearable devices, and the Internet of Things has inspired the relentless pursuit of microscale monolithic power sources (*1*–*3*). Among the numerous rechargeable energy storage systems reported to date, microsupercapacitors (MSCs) with in-plane interdigitated electrodes have received increasing attention as a promising candidate because of their efficient space utilization, device-customized integration, reliable electrochemical performance, and self-/wireless-powering electronics (*4*–*7*).

A foremost technical challenge facing MSCs is the reduction of feature size (i.e., electrode width) and gap between adjacent electrodes (*8*), which crucially affects the miniaturization, electrochemical kinetics, and areal energy density of the resulting MSCs. To address this issue, many previous studies relied on photolithography/selective etching (*4*, *5*, *9*–*14*) and laser scribing techniques (*15*). However, these often require complex/harsh processing conditions and hazardous materials, which hamper their practical application. As a facile approach to resolve this problem, an inkjet printing technique was explored (*16*–*22*); however, it has still suffered from low resolution (the smallest electrode width reported to date is limited to approximately 35 μm) (*16*). In addition to the feature size issue, the use of liquid electrolytes is another formidable challenge in the MSC development (*4*, *5*, *13*, *14*). The electrolyte leakage concern pushes the MSCs to the lack of design diversity, hampering their integration with electronic devices.

Here, we demonstrate a new class of ultrahigh areal number density solid-state MSCs (denoted as "UHD SS–MSCs") fabricated directly on a chip by electrohydrodynamic (EHD) jet printing. The on-chip UHD SS–MSCs comprise activated carbon-based, high-resolution interdigitated electrodes and ultraviolet (UV)–cured thermally/mechanically stable solid-state gel electrolytes. The details of the preparation and characteristics of the EHD jet-printed electrodes and solid-state gel electrolytes are described in subsequent sections. EHD jet printing, a state-of-the-art drop-on-demand printing technique (*23*–*25*), has recently drawn substantial attention as a high-resolution patterning technique in microelectronics. To the best of our knowledge, this is the first study to exploit EHD jet printing in the MSCs.

Benefiting from the process superiority and elaborately designed electrode/solid-state gel electrolyte, the on-chip UHD SS–MSCs offer (i) interdigitated electrodes with a fine feature size (electrode width = 10 μm), which is the smallest in the MSCs fabricated by printing techniques, (ii) on-demand (in-series/in-parallel) cell connection and highest areal number density [36 unit cells connected in series on a chip (area = 8.0 mm × 8.2 mm), 54.9 cells cm^{-2}], yielding an exceptionally high areal operating voltage (65.9 V cm^{-2}) that considerably exceeds those of previously reported MSCs fabricated by printing techniques, and (iii) reliable electrochemical performance under harsh operating conditions (e.g., exposure to mechanical vibration and high temperature).

RESULTS

Fabrication of on-chip UHD SS–MSCs via EHD jet printing

The overall fabrication of on-chip UHD SS–MSCs is schematically illustrated in Fig. 1A. On top of a titanium (Ti)/gold (Au) current collector of a silicon dioxide (SiO_2)/silicon (Si) chip substrate, nanosized activated carbon (nAC)–based electrode inks were deposited by EHD jet printing, creating high-resolution interdigitated electrodes with a fine feature size (10 μm) (Fig. 1, B and C). Subsequently, the solid-state gel electrolyte was introduced directly onto the electrodes through UV curing–assisted, EHD jet printing of the electrolyte ink. The UV curing allowed the solidification of the electrolyte ink via click reaction–based polymerization of the thiol-ene monomer mixture (*26*). The cross-sectional structure of the electrode-gel electrolyte assembly on the chip substrate, in which a vapor-deposited

[1]Department of Energy Engineering, School of Energy and Chemical Engineering, Ulsan National Institute of Science and Technology (UNIST), Ulsan 44919, Korea. [2]Department of Mechanical Engineering, Sungkyunkwan University, Suwon 16419, Korea. *Corresponding author. Email: syleek@unist.ac.kr

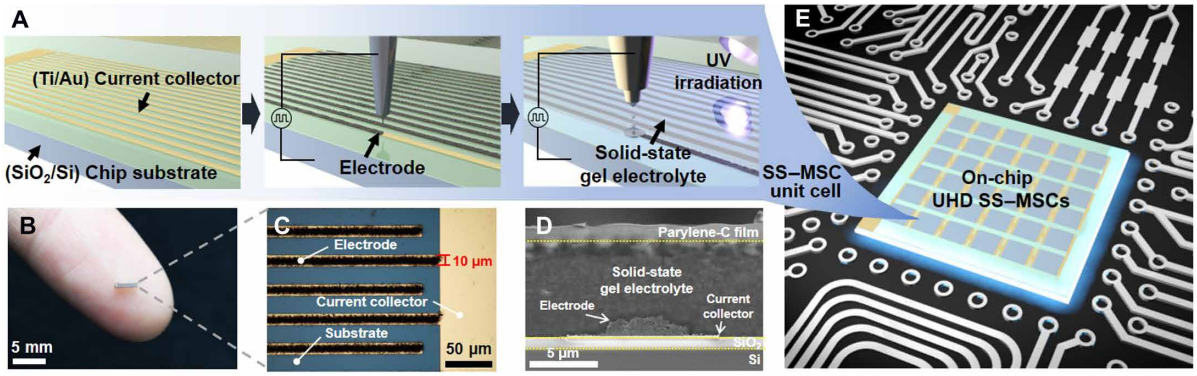

Fig. 1. Fabrication of on-chip UHD SS–MSCs via EHD jet printing. (**A**) Schematic representation depicting stepwise fabrication of the on-chip UHD SS–MSC. (**B**) Photograph of the SS–MSC on a human finger. (**C**) Optical microscopy image of the interdigitated electrodes (feature size = 10 μm) on the Ti/Au current collector. (**D**) Cross-sectional SEM image of the electrode/solid-state gel electrolyte assembly formed on the SiO_2/Si chip. (**E**) Conceptual illustration of the on-chip UHD SS–MSC monolithically integrated with the circuit board of an electronic device. Photo credit: (B) Kwon-Hyung Lee, Ulsan National Institute of Science and Technology.

parylene-C film was incorporated as a packaging substance, is shown in Fig. 1D. By repeating the fabrication process for the SS–MSC described above, we eventually developed on-chip UHD SS–MSCs, which can be monolithically integrated with a circuit board of an electronic device (Fig. 1E).

Design of electrode inks and fabrication of electrodes via EHD jet printing

A prerequisite for enabling stable drop-on-demand printing is preparing electrode inks with good dispersion and reliable processability. It is known that the particle size of the inks should be below 1/50 of the inner diameter of a printing nozzle to avoid nozzle clogging (*27*). Here, we used nAC particles with a mean diameter of 64.15 nm and a specific surface area of 1000 $m^2 g^{-1}$ (fig. S1), considering that a glass capillary nozzle with an inner diameter of 10 μm was installed in the EHD jet printing device. To ensure the colloidal dispersion stability of the electrode ink, carboxymethyl cellulose (CMC) was introduced as an electrode binder that can also tailor the surface charge of nAC particles. The other components of the electrode ink include carbon black particles (super-P) as a conductive additive and a ternary solvent mixture [comprising distilled water (DIW)/ethylene glycol (EG)/diethylene glycol (DEG)].

The dispersion state of the electrode ink, which critically affects the quality of printed electrodes, was investigated using zeta potential analysis. An electrostatically stable colloidal suspension normally has a zeta potential above ±30 mV (*28*) CMC, due to the presence of negatively charged carboxymethyl groups, enhanced the electrostatic repulsion between adjacent nAC particles in the electrode ink, yielding a zeta potential of −30.2 mV (Fig. 2A). A conceptual illustration showing the beneficial effect of CMC binder on the ink dispersion is displayed in Fig. 2B. The long-term dispersion stability of the electrode ink was evaluated by analyzing the UV–visible absorption spectra (Fig. 2C). No substantial change in the characteristic peak around 260 nm, assigned to an electronic transition between the π orbitals of carbon materials (*29*), was observed after 3 weeks, verifying the good dispersion stability of the electrode ink. Photographs of the electrode ink (initially and 3 weeks later) are provided as additional evidence (insets of Fig. 2C). The major physical properties (including the viscosity) of the electrode ink are described in fig. S2 (A and B). Meanwhile, a control electrode ink (without CMC binder) showed serious agglomeration, which was confirmed by a zeta potential of 9.53 mV and highly viscous/shear-thinning behavior (fig. S2, C to E).

In addition to the aforementioned ink design, control of processing parameters is important for high-fidelity EHD jet printing. As a case study, we investigated the effect of applied voltage (between a nozzle and a substrate) on the droplet size. Depending on the applied voltages, various EHD jetting modes, including Taylor cone, cone-jet, twin-jet, and multi-jet (*24*), are generated (top image of Fig. 2D). Figure 2D shows that the electrode inks were not ejected at applied voltages below 0.42 kV, where the electrostatic stress was not sufficiently high to overcome the surface tension of the ink. With applied voltages above 0.42 kV, the electrode ink was ejected from the apex of the Taylor cone (i.e., cone-jet mode), stably producing droplets with diameters of 8 to 10 μm. However, at excessively higher voltages, complex jetting modes (i.e., twin-jet and multi-jet) were observed, leading to an unwanted increase in droplet diameter and poor resolution. These results indicate that the preferred voltage for the cone-jet mode, which enables high resolution and a small feature size, is in the range of 0.42 to 0.44 kV. The other optimal processing parameters for the EHD jet-printed electrodes are summarized in fig. S3.

By exploiting the well-designed ink chemistry and processing conditions described above, we fabricated the interdigitated electrodes by EHD jet printing (movie S1). Note that the electrode width was approximately 10 μm, which is the smallest in the previously reported MSCs fabricated by printing techniques (table S1). Optical microscopy images and atomic force microscopy depth profiles showed that the electrode thickness tended to increase in proportion to the printing cycles, while the electrode width remained almost unchanged (Fig. 2E and fig. S4A), increasing the areal mass loading without impairing the printing resolution. This intriguing behavior may be attributed to Marangoni flow acceleration (*30*) in the printed droplets, which is generated by the surface tension gradient and the evaporation rate difference between the ternary solvents of the electrode ink. The surface tensions ($mN\ m^{-1}$)/boiling temperatures (°C) of the ternary solvents are 72.8/100 for water, 47.7/197.3 for EG, and 44.8/245 for DEG. The boosted Marangoni flow in the droplets can suppress an unwanted coffee-ring effect (commonly found in dried sessile droplets), enabling the electrode width to remain almost

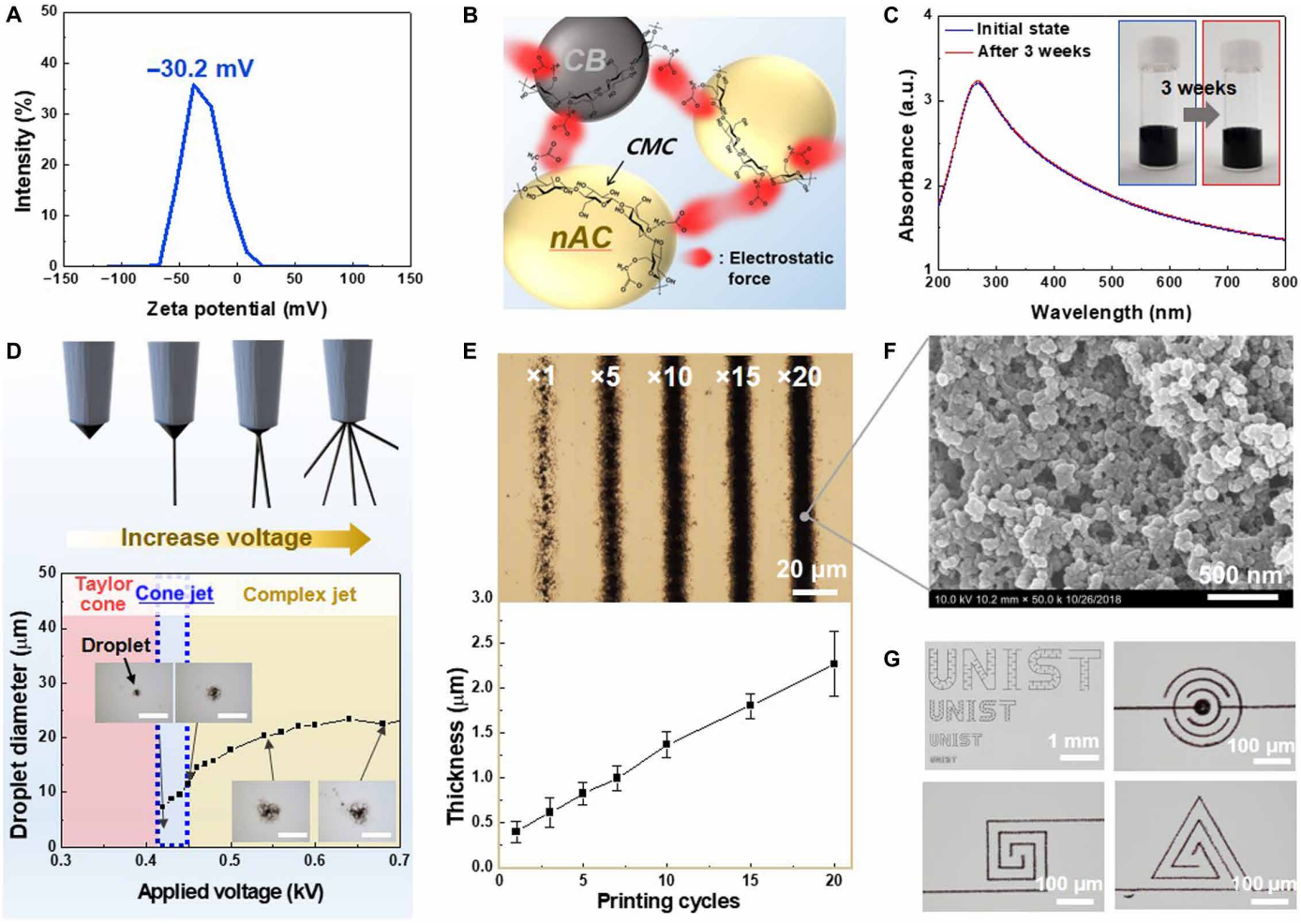

Fig. 2. Design of electrode inks and fabrication of electrodes via EHD jet printing. (**A**) Zeta potential profile of the electrode ink containing the CMC binder that acts as a surface charge–tuning agent of the nAC particles. (**B**) Schematic of the electrode ink representing the CMC-assisted electrostatic repulsion and its beneficial effect on the dispersion stability. (**C**) UV-vis absorption spectra and photographs (inset) of the electrode inks (initially and after 3 weeks). a.u., arbitrary units. (**D**) Conceptual depiction of various EHD jetting modes and change in the diameter of the ejected electrode droplets as a function of applied voltage. Insets are photographs of the droplets in different jetting modes. Scale bars, 20 μm. (**E**) Optical microscopy images and thickness variation of the electrodes as a function of printing cycles. (**F**) SEM image of the printed electrode (20 printing cycles). (**G**) Photographs of letter ("UNIST")-shaped printed electrodes of different sizes and micrometer-sized printed electrodes with various form factors. Photo credit: (C) Kwon-Hyung Lee, Ulsan National Institute of Science and Technology.

constant during the printing cycles. In addition, the electrodes exhibited the gradual increase of areal capacitance with increasing the printing cycles (fig. S4B). Moreover, no dimensional disruption was observed even after being washed by the flowing solvents (fig. S4C), demonstrating the structural stability of the electrodes.

Morphological analysis of the printed electrode (20 printing cycles) showed that the nAC particles, along with the carbon black conductive additives, are uniformly dispersed and highly interconnected (Fig. 2F). Such a well-percolated network beneficially contributes to high electronic conductivity (11.1 S cm^{-1}) of the printed electrode. Figure 2G shows that letter ("UNIST")-shaped electrodes of different sizes (ranging from the micrometer to millimeter scale) were prepared by EHD jet printing. In addition, the micrometer-sized electrodes with various form factors (including interdigitated circle, twisted square, and spiral triangle) were successfully fabricated, demonstrating the aesthetic diversity of the EHD jet-printed electrodes.

Solid-state gel electrolytes fabricated via UV curing–assisted EHD jet printing

To enable compact integration of SS–MSCs unit cells and their on-demand (in-series/in-parallel) connection in a confined area, electrochemical isolation between the unit cells should be ensured as an essential prerequisite. Conventional liquid electrolytes often fail to meet this requirement due to their fluidic characteristic. To address this issue, Hata *et al.* (*14*) reported photocured hydrophobic barriers. However, complex manufacturing processes were required to fabricate the barriers and other cell components. Moreover, a volatile aqueous liquid electrolyte was used, which may impair the thermal tolerance and dimensional stability of the resulting MSC.

Here, we introduced a solid-state gel electrolyte directly onto the prefabricated interdigitated electrodes via drying-free, UV curing–assisted EHD jet printing. The electrolyte ink (i.e., before UV curing) showed Newtonian fluid behavior, which is desirable for EHD jet printing (fig. S5A). The optimal processing parameters for the

electrolyte preparation are provided in fig. S5B. After exposure to UV irradiation, the electrolyte ink was solidified to form a self-standing gel electrolyte film. The fabrication of the solid-state gel electrolyte is schematically shown in Fig. 3A, where the UV-induced click reaction of thiol-ene monomer mixture with trimethylolpropane tris(3-mercaptopropionate) (TMPTMP, thiol monomer) and trimethylolpropane triacrylate (TMPTA, ene monomer) was conducted in the presence of ionic liquid (1-ethyl-3-methylimidazolum bis (trifluoromethylsulfonyl)imide, [EMIM][TFSI]). The composition ratio of the [EMIM][TFSI] and thiol-ene monomer mixture [TMPTMP/TMPTA = 1/2 (mol/mol)] was 85/15 (w/w). Notably, no traditional processing solvents such as water, acetone, or *N*-methyl-2-pyrrolidone were used, indicating that the solid-state gel electrolyte can be simply fabricated without solvent-drying steps. Meanwhile, the UV curing–assisted synthesis of the thiol-ene polymer network skeleton was verified by the changes in the Fourier transform infrared (FTIR) spectroscopy peaks assigned to thiol (—SH) groups (2575 cm^{-1}) (*31*) and acrylic C═C bonds (1610 to 1625 cm^{-1}) (Fig. 3B) (*32*) and the viscoelastic properties (fig. S6A).

A beneficial role of the solid-state gel electrolyte in fabricating on-chip UHD SS–MSCs was explored. The solid-state gel electrolyte and liquid electrolyte ([EMIM][TFSI] alone, as a control sample) were printed in the form of pixel arrays (area of a pixel = 0.8 mm × 0.8 mm) on a SiO_2/Si chip substrate. Figure 3C shows that the solid-state gel electrolyte pixel arrays preserved their shape and dimensions even after being subjected to mechanical vibration. By comparison, significant flooding and crossover between the liquid electrolyte pixel arrays were observed, indicating that the liquid electrolyte may be unsuitable for securing electrochemical isolation between the unit cells.

The solid-state gel electrolyte showed a gradual increase in ionic conductivity with temperature, along with acceptable ionic conductivity (2.62×10^{-3} S cm^{-1}) at room temperature (Fig. 3D). Meanwhile, a supplementary experiment was conducted with model cells to address a concern on the electrolyte-electrode wettability. Details on the cell fabrication were described in the experimental section. No significant difference in the cyclic voltammetry (CV) profiles was observed between the solid-state gel electrolyte and liquid electrolyte (fig. S6B). This result indicates the nAC electrodes were well wetted with the electrolyte ink, underscoring a unique feature of the solid-state electrolyte (i.e., fluidic ink before UV curing ➔ solidified film after UV curing).

In addition, because of the thermally tolerant [EMIM][TFSI] and thiol-ene polymer network skeleton, the solid-state gel electrolyte showed stable ionic conductivity at a high temperature of 150°C, and its dimensions were almost unchanged after 120 min (Fig. 3E). In contrast, a H_3PO_4/polyvinyl alcohol polymer electrolyte (chosen as a control sample), which has been widely used in previously reported SS–MSCs (*19*–*21*), was thermally damaged after only 10 min and was significantly shrunken after 30 min. Furthermore, the

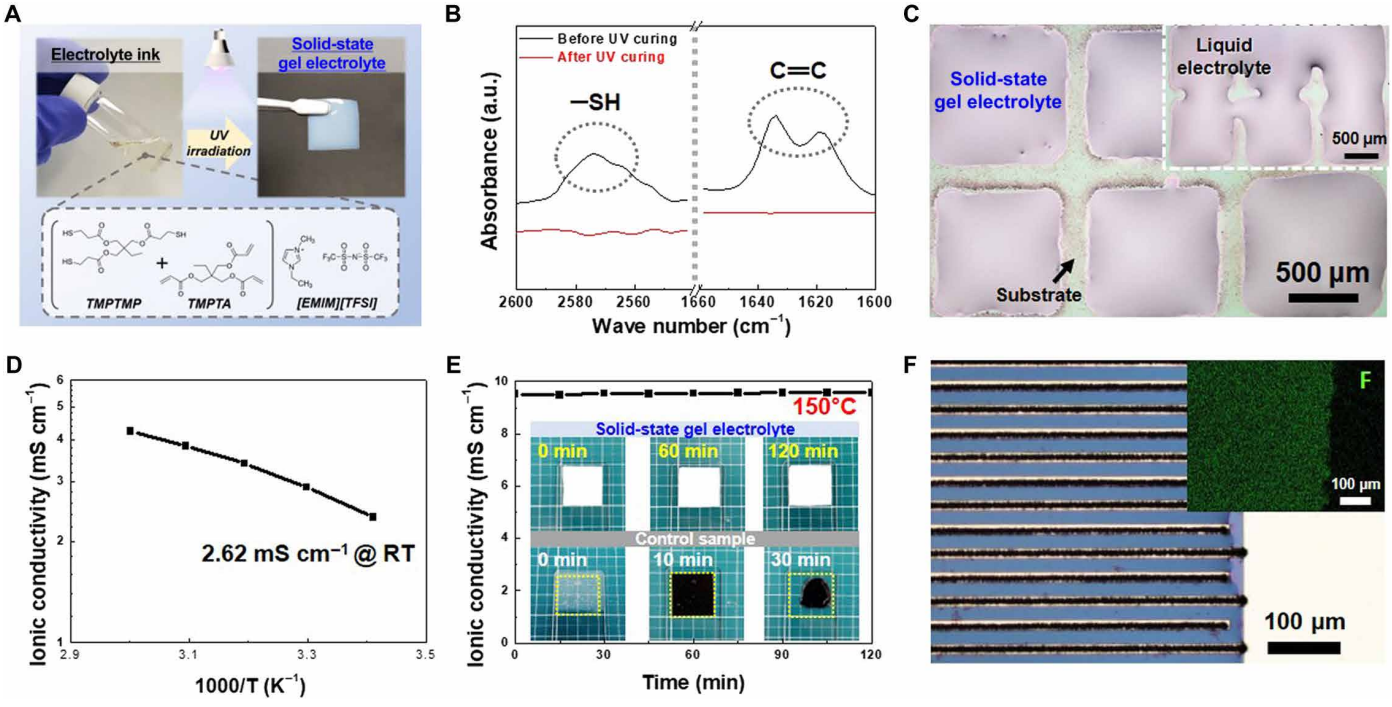

Fig. 3. Solid-state gel electrolytes fabricated via UV curing–assisted EHD jet printing. (**A**) Schematic representation depicting preparation of the solid-state gel electrolyte, along with the chemical structures of the electrolyte components. (**B**) Change in the characteristic FTIR peaks assigned to thiol (—SH) groups (2575 cm^{-1}) and acrylic C═C bonds (1610 to 1625 cm^{-1}) in the thiol-ene polymer network before/after UV curing. (**C**) Optical microscopy image of the solid-state gel electrolyte–deposited pixel arrays (area of a pixel = 0.8 mm × 0.8 mm) after being subjected to mechanical vibration for 60 s (vortex mixer; amplitude, 3 mm; frequency, 2000 Hz). Inset shows the liquid electrolyte (i.e., [EMIM][TFSI]) pixel arrays. (**D**) Ionic conductivity of the solid-state gel electrolyte as a function of temperature. RT, room temperature, 25°C. (**E**) Change in the ionic conductivity and dimensions of the solid-state gel electrolyte at 150°C as a function of elapsed time. (**F**) Optical microscopy image of the solid-state gel electrolyte fabricated directly on the interdigitated electrode-deposited SiO_2/Si chip substrate via EHD jet printing. Inset shows an EDS elemental mapping image showing uniform coverage of the interdigitated electrodes with the solid-state gel electrolyte, in which the green dots represent fluorine atoms originating from the [EMIM][TFSI] ionic liquid. Photo credit: (A and E) Kwon-Hyung Lee, Ulsan National Institute of Science and Technology.

solid-state gel electrolyte maintained its ionic conductivity and dimensional integrity in a vacuum state (pressure < 10^{-2} Pa) (fig. S6, C and D). The thermal stability and vacuum tolerance of the solid-state gel electrolyte are expected to allow process combination of EHD printing with traditional chip fabrication techniques (requiring harsh fabrication steps including evaporation, sputtering, and thermal treatment), eventually enabling seamless unitization of UHD SS–MSCs with a chip.

Before electrolyte printing, the SiO_2/Si chip substrate was subjected to UV-ozone (UVO) treatment to achieve good affinity with the electrolyte ink. The UVO treatment decreased the contact angle of the electrolyte ink on the SiO_2/Si chip substrate (fig. S7, A and B): 37.6° (before UVO treatment) to 20.7° (after). Note that the UVO-treated SiO_2/Si chip substrate allowed stable electrolyte ink deposition, in comparison with the pristine SiO_2/Si chip substrate which showed randomly deposited, island-like electrolyte ink (fig. S7, C and D). Consequently, the solid-state gel electrolyte was successfully printed on the interdigitated electrode-deposited SiO_2/Si chip substrate (Fig. 3F and movie S2). Complete/uniform coverage with the solid-state gel electrolyte was verified by an energy dispersive x-ray spectroscopy (EDS) elemental mapping image (inset of Fig. 3F), in which green dots represent fluorine atoms originating from the [EMIM][TFSI] ionic liquid.

Fabrication and electrochemical characterization of SS–MSCs

The interdigitated electrode dimensions crucially affect the electrochemical kinetics of in-plane MSCs (*20*). To date, systematic

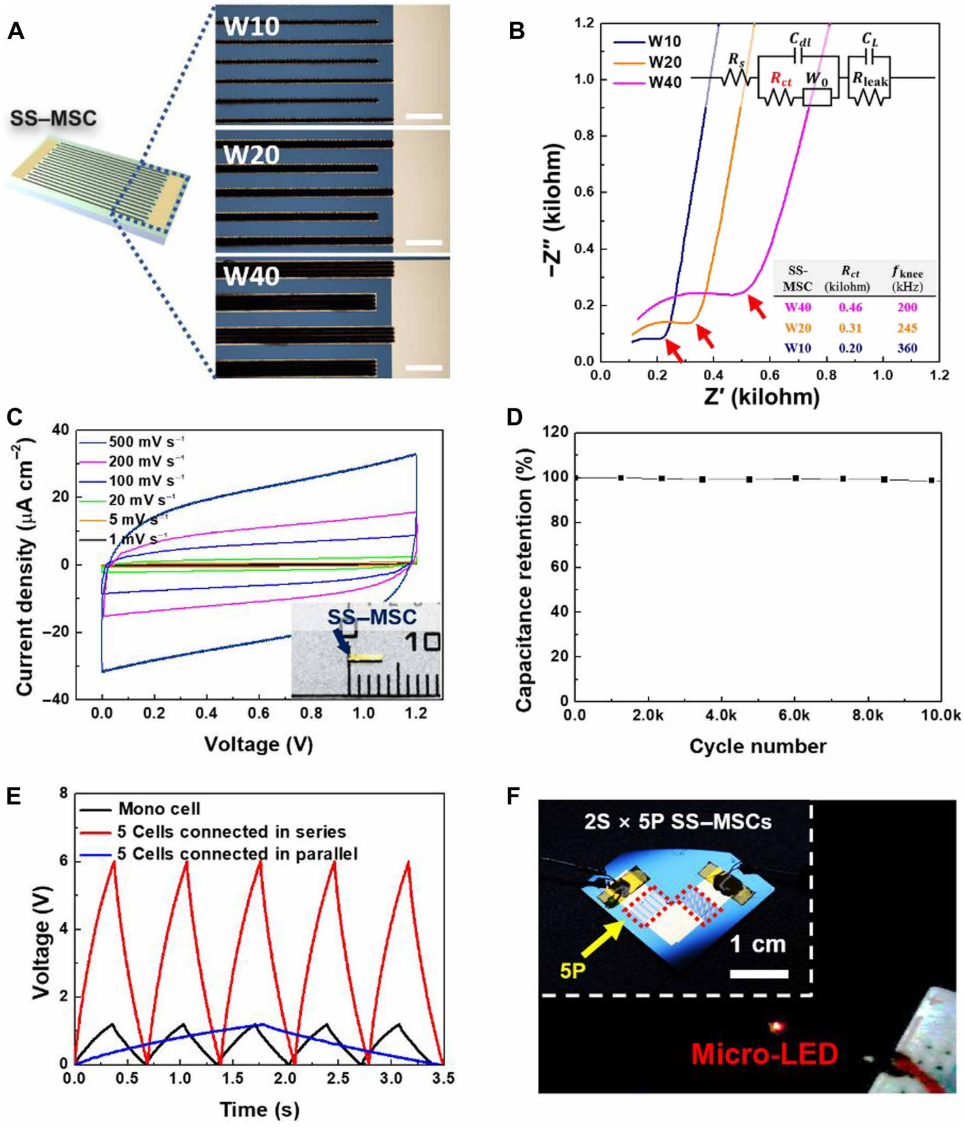

Fig. 4. Electrochemical performance of SS–MSCs. (**A**) Optical microscopy images of the printed electrodes with different widths (10, 20, and 40 μm, denoted as W10, W20, and W40, respectively). Scale bars, 50 μm. (**B**) Nyquist plots of the SS–MSCs with different electrode widths. Inset shows an associated equivalent circuit based on a modified Randles circuit. Red arrows indicate knee frequencies. (**C**) CV profiles (scan rate, 1 to 500 mV s^{-1}) of the SS–MSC. Inset shows a photograph of the SS–MSC. (**D**) Capacitance retention (scan rate, 1000 mV s^{-1}) of the SS–MSC as a function of charge/discharge cycle number. (**E**) Galvanostatic charge-discharge (GCD) profiles of the five SS–MSC unit cells connected in series or in parallel. (**F**) Photograph of the micro–light emitting diode (LED) powered by 10 SS–MSC unit cells with the combined configuration (2S × 5P) of two cells in series (2S) and five cells in parallel (5P, represented by the red dashed boxes). Photo credit: (F) Kwon-Hyung Lee, Ulsan National Institute of Science and Technology.

investigation of the MSC performance has been limited to electrode widths above 50 μm (*33*). Here, the effect of electrode width on the electrochemical performance of the SS–MSCs was examined, with a focus on narrow electrode widths (<50 μm). A series of SS–MSCs with different electrode widths (10, 20, and 40 μm, denoted as W10, W20, and W40, respectively) (Fig. 4A) were prepared using EHD jet printing, where the other cell dimensions were fixed (fig. S8, A and B). An electrode width below 10 μm was difficult to achieve at this stage, and this will be investigated in our future studies. Nyquist plots of the resulting SS–MSCs are shown in Fig. 4B, with an associated equivalent circuit based on a modified Randles circuit (*34*). The radius of a semicircle, which represents ion diffusion resistance in electrodes (*35*), tended to decrease (0.46, 0.31, and 0.20 kilohm) as the electrode width decreased, revealing the advantageous effect of the narrow electrode width on the ion diffusion kinetics. In addition, the higher knee frequency at the narrower electrode width reveals fast frequency response.

On the basis of this understanding of the electrode width, we fabricated a SS–MSC unit cell (area = 0.5 mm × 3.5 mm) with an electrode width of 10 μm (inset of Fig. 4C). CV profiles of the unit cell (Fig. 4C) showed normal capacitive behavior over a wide range of scan rates (1 to 500 mV s^{-1}). The areal capacitance (at a scan rate of 1 mV s^{-1}) of the unit cell was estimated as 127.5 μF cm^{-2}, which appeared comparable with those of previously reported carbon-based thin-film MSCs (*9*, *10*, *19*). Meanwhile, the capacitance of a bare Ti/Au current collector itself was negligibly small (fig. S8C), verifying the predominant contribution of nAC active materials to the unit cell capacitance. A galvanostatic charge-discharge (GCD) test (at areal current densities of 1.30 to 27.78 μA cm^{-2}) showed typical linear voltage-time profiles with high coulombic efficiency (fig. S8, D and E). In addition, the SS–MSC presented stable capacity retention over 10,000 cycles (Fig. 4D).

SS–MSCs with on-demand (in-series/in-parallel) cell configurations were developed. Five SS–MSC unit cells were connected in series or in parallel (fig. S9), leading to a fivefold increase in the voltage (in-series connection) or capacitance (in-parallel connection) (Fig. 4E). Notably, 10 SS–MSC unit cells with a combined configuration (2S × 5P) of two cells in series (2S) and five cells in parallel (5P) were fabricated. They successfully lit up a micro–light emitting diode (LED) (Fig. 4F), demonstrating customized control of the cell voltage and capacitance.

On-chip UHD SS–MSCs as a device-unitized power source

To further highlight the architectural/electrochemical uniqueness of the EHD jet-printed SS–MSCs, UHD SS–MSCs, comprising 36 unit cells connected in series, were fabricated on a chip (area = 8.0 mm × 8.2 mm, smaller than a coin) (Fig. 5A). Note that this high areal number density (54.9 cells cm^{-2}) of the UHD SS–MSCs far exceeds those of previously reported MSCs fabricated by printing techniques (table S1).

To explore their potential application as a device-unitized power source, the on-chip UHD SS–MSCs were monolithically integrated with a circuit board (Fig. 5B). A series of CVs were estimated at an interval of 5.0 V (the last interval was 3.2 V) at a scan rate of 1.0 V s^{-1} under ambient measurement conditions. Figure 5C shows a stepwise increase in the cell voltage, along with normal capacitive behavior over the whole voltage range. Notably, the on-chip UHD SS–MSCs [36 unit cells connected in-series on a chip (area = 8.0 mm × 8.2 mm)]

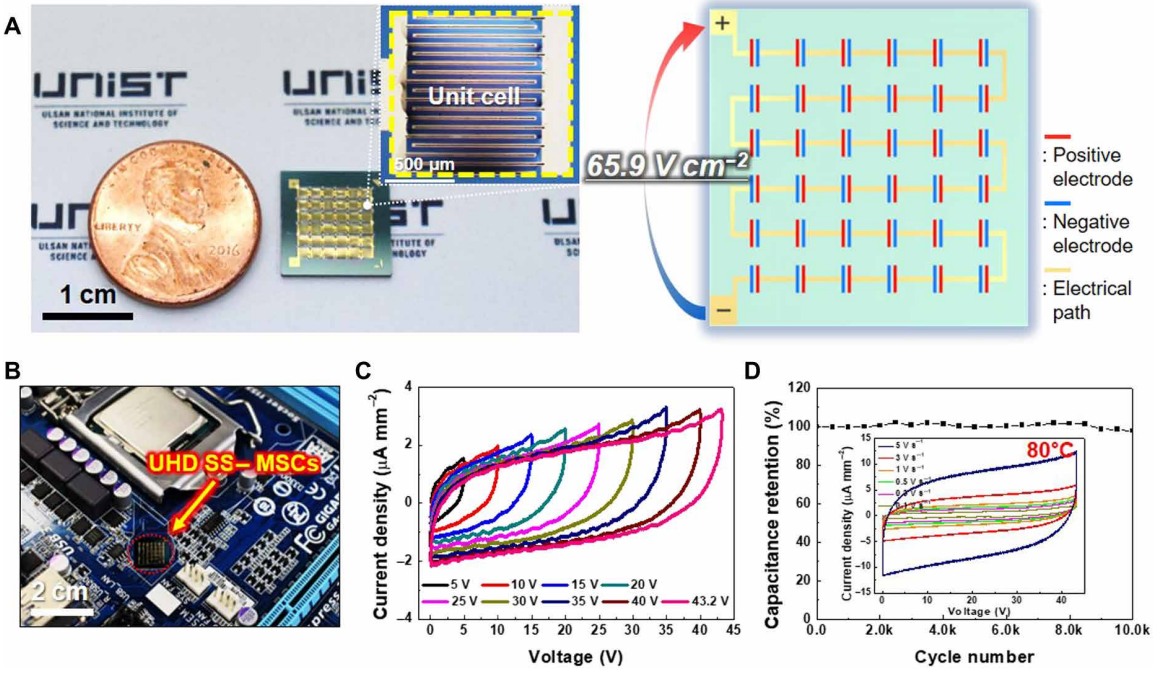

Fig. 5. On-chip UHD SS–MSCs as a device-unitized power source. (**A**) Photographs and schematic representation of the UHD SS–MSCs (comprising 36 unit cells connected in series) fabricated on a chip (area = 8.0 mm × 8.2 mm, smaller than a coin). Inset shows an optical microscopy image of the unit cell in the UHD SS–MSCs. (**B**) Photograph of the on-chip UHD SS–MSCs monolithically integrated on a circuit board of an electronic device. (**C**) A series of CV profiles (scan rate, 1 V s^{-1}) of the on-chip UHD SS–MSCs in the voltage range 5 to 43.2 V at an interval of 5.0 V (the last interval was 3.2 V). (**D**) Capacitance retention (scan rate, 20.0 V s^{-1}) of the on-chip UHD SS–MSCs as a function of charge/discharge cycle number at an areal operating voltage of 65.9 V cm^{-2}. Inset shows CV profiles over a wide range of scan rates (0.1 to 5.0 V s^{-1}) after exposure to a hot plate (80°C) for 0.5 hours. Photo credit: (A and B) Kwon-Hyung Lee, Ulsan National Institute of Science and Technology.

reached a high cell voltage of 43.2 V, which corresponds to an exceptional areal operating voltage of 65.9 V cm^{-2}. Such a high areal operating voltage has been never reported in the printed MSCs (table S1). These unusual characteristics were further highlighted by estimating the volume-based device performance. The on-chip UHD SS–MSCs showed the significantly high volumetric number density (1026 cells cm^{-3}) and volumetric operating voltage (1232 V cm^{-3}), in which their volume was determined by considering all components (including the chip substrate, current collector, electrode, solid-state gel electrolyte, and packaging substance). The on-chip UHD SS–MSCs exhibited stable capacity retention over 10,000 cycles even under a high areal operating voltage of 65.9 V cm^{-2} (Fig. 5D). To explore the temperature tolerance of the UHD SS–MSCs, their stability against thermal shock was investigated. Upon exposure to a hot plate (80°C), the UHD SS–MSCs maintained normal CV profiles over a wide range of scan rates (0.1 to 5.0 V s^{-1}) (inset of Fig. 5D).

DISCUSSION

We have demonstrated on-chip UHD SS–MSCs fabricated via EHD jet printing. As a prerequisite step for successful EHD jet printing, the electrode and electrolyte inks were elaborately prepared, with a particular focus on the dispersion state, processing requirements, and rheological/electrochemical properties. The CMC-mediated electrostatic repulsion between the nAC particles improved the dispersion stability of the electrode ink, contributing to fabrication of interdigitated electrodes with a fine feature size (electrode width = 10 μm). The solid-state gel electrolyte was introduced directly onto the electrodes through drying-free, UV curing-assisted EHD jet printing. Due to its structural integrity and thermal tolerance, the solid-state gel electrolyte allowed electrochemical isolation between the SS–MSCs and process combination with traditional chip fabrication, resulting in dense integration of SS–MSCs with on-demand (in-series/in-parallel) connection on a chip. Driven by the process novelty and rational design of the electrode/electrolyte, the resulting on-chip UHD SS–MSCs exhibited the exceptionally high areal number density (36 unit cells on a chip (area = 8.0 mm × 8.2 mm, 54.9 cells cm^{-2}) and areal operating voltage (65.9 V cm^{-2}) that lie far beyond those of previously reported MSCs fabricated by printing techniques. The on-chip UHD SS–MSCs presented here hold great promise as a new platform technology for miniaturized monolithic power sources with customized design and tunable electrochemical properties.

MATERIALS AND METHODS

Preparation of the electrode and electrolyte inks

To prepare the electrode ink, nAC particles (average diameter = 64.15 nm; Akzo Nobel) and carbon black conductive additives (super-P) were mixed in a solution [CMC binder-dissolved ternary solvent mixture of DIW/EG/DEG = 1/1/1 (w/w/w)] using a planetary mixer (ARE-310, Thinky), in which the weight-based composition ratio was nAC/CMC/super-P = 66.8/25.0/8.2 (w/w/w). After bath sonication for 1 hour, the suspension was subjected to centrifugation (at 10,000*g* for 1 hour) and went through a syringe filter (pore size, 0.1 μm) to remove large-size agglomerates. Meanwhile, to prepare the electrolyte ink, an ionic liquid ([EMIM][TFSI]) was mixed with UV-curable thiol-ene monomer mixtures (consisting of TMPTMP/TMPTA = 1/2 (mol/mol), 1.0 weight % of 2,2-dimethoxy-2-phenylacetophenone was incorporated as a photoinitiator), in which the composition ratio of the electrolyte ink was [EMIM][TFSI]/monomer mixture = 85/15 (w/w).

Fabrication of the on-chip UHD SS–MSCs

The on-chip UHD SS–MSCs were fabricated using a multifunctional EHD jet printing system (Enjet Inc.). As a chip substrate for the UHD SS–MSCs, a piece of silicon wafer with a thermally grown 1-μm-thick SiO_2 top layer was used. Onto the SiO_2/Si chip substrate, metal current collectors [Ti (10 nm)/Au (100 nm)] were fabricated using a conventional nanofabrication technique (*36*). On top of the metal current collector, the electrode ink was EHD jet–printed through a glass capillary nozzle (inner diameter = 10 μm) and then dried in a vacuum oven at 50°C for 1 hour, yielding the electrodes with interdigitated configuration. Then, the electrode-printed chip substrate was subjected to UVO treatment for 10 min (UVC-30, Jaesung Engineering Co.). Subsequently, the electrolyte ink was printed on the interdigitated electrodes through the EHD jet printing. To solidify the electrolyte ink, the UV irradiation (Hg UV lamp; peak intensity = 5000 mW cm^{-2}; Lichtzen) was exploited. By repeatedly conducting the printing/UV curing process of the SS–MSC described above, we fabricated the on-chip UHD SS–MSCs. Last, the electrode/electrolyte assembly was sealed with a parylene-C film (used as a packaging substance) using a vapor deposition system (Alpha plus). The model cells used to investigate electrolyte-electrode wettability were fabricated using 2032-type coin cells with two-electrode configuration [= nAC electrode/solid-state gel electrolyte (or liquid electrolyte soaked polypropylene separator)/nAC electrode], in which the nAC electrode was fabricated by casting the electrode slurry mixture [nAC/carbon black/CMC = 66.8/25.0/8.2 (w/w/w) in water] on a Ni foil current collector and followed by drying at 60°C for 12 hours in a vacuum oven.

Characterization of cell components, SS–MSCs, and UHD SS–MSCs

The surface charge (zeta potential) of the nAC particles in the electrode ink was characterized with a ZetaSizer (Nano ZS, Malvern Panalytical). The specific surface area of the nAC particles was analyzed with N_2 adsorption-desorption isotherms at 77 K using physisorption analyzer ASAP2020 (Micromeritics). The physical appearance of the cell components, SS–MSC and UHD SS–MSCs, were characterized using an optical microscope (LV100ND, Nikon). The surface and cross-sectional morphologies of the EHD jet-printed interdigitated electrodes and electrode-gel electrolyte assembly were investigated by atomic force microscopy (DI-3100, Veeco) and field emission scanning electron microscopy (s-4800, Hitachi). The dispersion stability of the electrode ink was examined using UV-vis spectroscopy (Cary 5000, Agilent). The rheological properties of the electrode/electrolyte inks were characterized using a rheometer (Haake MARS III, Thermo Electron GmbH). The surface tension and electrolyte contact angle of the SiO_2/Si chip substrate were measured using a drop shape analyzer (Phoenix 300, SEO). The electrical resistances of the printed electrodes were estimated using four-point probe measurement (CMT-SR1000N, Advanced Instrument Technology). The UV-curing reaction of the solid-state gel electrolyte was examined using an FTIR spectrometer (Alpha Platinum ATR, Bruker) with a spectral resolution of 4 cm^{-1}. The ionic conductivity of the solid-state gel electrolyte was estimated by analyzing the AC impedance over the frequency range from 10^{-1} to 10^{6} Hz

with a perturbation of 14.2 mV in a temperature range from 20° to 60°C. The electrochemical performances of the SS–MSCs and UHD SS–MSCs were measured using a potentiostat/galvanostat (VMP-300, Bio-Logic) equipped with a 48-V voltage booster. The areal number density and areal operating voltage were calculated by the following equations

Areal number density

$$(\text{cells cm}^{-2}) = \frac{\text{total number of unit cells}(= 36\text{cells})}{\text{chip area}(= 0.656\,\text{cm}^2)} \quad (1)$$

Areal operating voltage

$$(\text{V cm}^{-2}) = \frac{\text{operating voltage of the UHD–MSCs}(= 43.2\text{V})}{\text{chip area}(= 0.656\,\text{cm}^2)} \quad (2)$$

SUPPLEMENTARY MATERIALS

Supplementary material for this article is available at http://advances.sciencemag.org/cgi/content/full/6/10/eaaz1692/DC1

Fig. S1. Basic characteristics of nAC.
Fig. S2. Characteristics of the electrode ink with and without CMC binder.
Fig. S3. Process description of the EHD jet printing for the fabrication of interdigitated electrodes.
Fig. S4. Characterization of the EHD jet-printed electrodes as a function of printing cycles.
Fig. S5. EHD jet printing of the electrolyte ink.
Fig. S6. Characteristics of the solid-state gel electrolytes.
Fig. S7. Photographs showing contact angle change and effect on the affinity between the electrolyte ink and SiO_2/Si chip substrate.
Fig. S8. Configuration and electrochemical performance of the SS–MSC.
Fig. S9. Schematic representation of the five SS–MSCs.
Table S1. Comparison in the major characteristics between the on-chip UHD SS–MSCs (this study) and the previously reported MSCs fabricated by printing techniques.
Movie S1. Video clip showing the fabrication of interdigitated electrodes on top of the SiO_2/Si chip substrate through the EHD jet printing.
Movie S2. Video clip showing the fabrication of solid-state gel electrolytes on top of interdigitated electrodes-deposited SiO_2/Si chip substrate through the EHD jet printing.
References (*37*–*40*)

REFERENCES AND NOTES

1. N. A. Kyeremateng, T. Brousse, D. Pech, Microsupercapacitors as miniaturized energy-storage components for on-chip electronics. *Nat. Nanotechnol.* **12**, 7–15 (2017).
2. M. Beidaghi, Y. Gogotsi, Capacitive energy storage in micro-scale devices: Recent advances in design and fabrication of micro-supercapacitors. *Energ. Environ. Sci.* **7**, 867–884 (2014).
3. L. Liu, Q. Weng, X. Lu, X. Sun, L. Zhang, O. G. Schmidt, Advances on microsized on-chip lithium-ion batteries. *Small* **13**, 1701847 (2017).
4. J. Chmiola, C. Largeot, P.-L. Taberna, P. Simon, Y. Gogotsi, Monolithic carbide-derived carbon films for micro-supercapacitors. *Science* **328**, 480–483 (2010).
5. P. Huang, C. Lethien, S. Pinaud, K. Brousse, R. Laloo, V. Turq, M. Respaud, A. Demortière, B. Daffos, P. L. Taberna, B. Chaudret, Y. Gogotsi, P. Simon, On-chip and freestanding elastic carbon films for micro-supercapacitors. *Science* **351**, 691–695 (2016).
6. C. Zhao, Y. Liu, S. Beirne, J. Razal, J. Chen, Recent development of fabricating flexible micro-supercapacitors for wearable devices. *Adv. Mater. Technol.* **3**, 1800028 (2018).
7. C. Shen, S. Xu, Y. Xie, M. Sanghadasa, X. Wang, L. Lin, A review of on-chip micro supercapacitors for integrated self-powering systems. *J. Microelectromech. Syst.* **26**, 949–965 (2017).
8. H. Li, J. Liang, Recent development of printed micro-supercapacitors: Printable materials, printing technologies, and perspectives. *Adv. Mater.* **32**, 1805864 (2019).
9. Z.-S. Wu, K. Parvez, X. Feng, K. Müllen, Graphene-based in-plane micro-supercapacitors with high power and energy densities. *Nat. Commun.* **4**, 2487 (2013).
10. Z.-S. Wu, K. Parvez, X. Feng, K. Müllen, Photolithographic fabrication of high-performance all-solid-state graphene-based planar micro-supercapacitors with different interdigital fingers. *J. Mater. Chem. A* **2**, 8288–8293 (2014).
11. Z.-S. Wu, K. Parvez, S. Li, S. Yang, Z. Liu, S. Liu, X. Feng, K. Müllen, Alternating stacked graphene-conducting polymer compact films with ultrahigh areal and volumetric capacitances for high-energy micro-supercapacitors. *Adv. Mater.* **27**, 4054–4061 (2015).
12. Z. Niu, L. Zhang, L. Liu, B. Zhu, H. Dong, X. Chen, All-solid-state flexible ultrathin micro-supercapacitors based on graphene. *Adv. Mater.* **25**, 4035–4042 (2013).
13. M. Beidaghi, C. Wang, Micro-supercapacitors based on interdigital electrodes of reduced graphene oxide and carbon nanotube composites with ultrahigh power handling performance. *Adv. Funct. Mater.* **22**, 4501–4510 (2012).
14. K. U. Laszczyk, K. Kobashi, S. Sakurai, A. Sekiguchi, D. N. Futaba, T. Yamada, K. Hata, Lithographically integrated microsupercapacitors for compact, high performance, and designable energy circuits. *Adv. Energy Mater.* **5**, 1500741 (2015).
15. M. F. El-Kady, R. B. Kaner, Scalable fabrication of high-power graphene micro-supercapacitors for flexible and on-chip energy storage. *Nat. Commun.* **4**, 1475 (2013).
16. Y. Lin, Y. Gao, Z. Fan, Printable fabrication of nanocoral-structured electrodes for high-performance flexible and planar supercapacitor with artistic design. *Adv. Mater.* **29**, 1701736 (2017).
17. Z. Liu, Z.-S. Wu, S. Yang, R. Dong, X. Feng, K. Müllen, Ultraflexible in-plane micro-supercapacitors by direct printing of solution-processable electrochemically exfoliated graphene. *Adv. Mater.* **28**, 2217–2222 (2016).
18. Y. Wang, Y.-Z. Zhang, D. Dubbink, J. E. ten Elshof, Inkjet printing of δ-MnO 2 nanosheets for flexible solid-state micro-supercapacitor. *Nano Energy* **49**, 481–488 (2018).
19. J. Li, V. Mishukova, M. Östling, All-solid-state micro-supercapacitors based on inkjet printed graphene electrodes. *Appl. Phy. Lett.* **109**, 123901 (2016).
20. W. Liu, C. Lu, H. Li, R. Y. Tay, L. Sun, X. Wang, W. L. Chow, X. Wang, B. K. Tay, Z. Chen, J. Yan, K. Feng, G. Lui, R. Tjandra, L. Rasenthiram, G. Chiu, A. Yu, Paper-based all-solid-state flexible micro-supercapacitors with ultra-high rate and rapid frequency response capabilities. *J. Mater. Chem. A* **4**, 3754–3764 (2016).
21. L. Li, E. B. Secor, K.-S. Chen, J. Zhu, X. Liu, T. Z. Gao, J.-W. T. Seo, Y. Zhao, M. C. Hersam, High-performance solid-state supercapacitors and microsupercapacitors derived from printable graphene inks. *Adv. Energy Mater.* **6**, 1600909 (2016).
22. K.-H. Choi, J. Yoo, C. K. Lee, S.-Y. Lee, All-inkjet-printed, solid-state flexible supercapacitors on paper. *Energ. Environ. Sci.* **9**, 2812–2821 (2016).
23. J.-U. Park, M. Hardy, S. J. Kang, K. Barton, K. Adair, D. K. Mukhopadhyay, C. Y. Lee, M. S. Strano, A. G. Alleyne, J. G. Georgiadis, P. M. Ferreira, J. A. Rogers, High-resolution electrohydrodynamic jet printing. *Nat. Mater.* **6**, 782–789 (2007).
24. M. S. Onses, E. Sutanto, P. M. Ferreira, A. G. Alleyne, J. A. Rogers, Mechanisms, capabilities, and applications of high-resolution electrohydrodynamic jet printing. *Small* **11**, 4237–4266 (2015).
25. Q. Huang, Y. Zhu, Printing conductive nanomaterials for flexible and stretchable electronics: A review of materials, processes, and applications. *Adv. Mater. Technol.* **4**, 1800546 (2019).
26. C. E. Hoyle, A. B. Lowe, C. N. Bowman, Thiol-click chemistry: A multifaceted toolbox for small molecule and polymer synthesis. *Chem. Soc. Rev.* **39**, 1355–1387 (2010).
27. G. Hu, J. Kang, L. W. T. Ng, X. Zhu, R. C. T. Howe, C. G. Jones, M. C. Hersam, T. Hasan, Functional inks and printing of two-dimensional materials. *Chem. Soc. Rev.* **47**, 3265–3300 (2018).
28. J. Jiang, G. Oberdörster, P. Biswas, Characterization of size, surface charge, and agglomeration state of nanoparticle dispersions for toxicological studies. *J. Nanopart. Res.* **11**, 77–89 (2008).
29. M. Sharif Sh, F. Golestani Fard, E. Khatibi, H. Sarpoolaky, Dispersion and stability of carbon black nanoparticles, studied by ultraviolet–visible spectroscopy. *J. Taiwan Inst. Chem. Eng.* **40**, 524–527 (2009).
30. M. Kuang, L. Wang, Y. Song, Controllable printing droplets for high-resolution patterns. *Adv. Mater.* **26**, 6950–6958 (2014).
31. M. Willgert, M. H. Kjell, G. Lindbergh, M. Johansson, New structural lithium battery electrolytes using thiol–ene chemistry. *Solid State Ion.* **236**, 22–29 (2013).
32. E.-H. Kil, K. H. Choi, H. J. Ha, S. Xu, J. A. Rogers, M. R. Kim, Y.-G. Lee, K. M. Kim, K. Y. Cho, S.-Y. Lee, Imprintable, bendable, and shape-conformable polymer electrolytes for versatile-shaped lithium-ion batteries. *Adv. Mater.* **25**, 1395–1400 (2013).
33. D. Pech, M. Brunet, T. M. Dinh, K. Armstrong, J. Gaudet, D. Guay, Influence of the configuration in planar interdigitated electrochemical micro-capacitors. *J. Power Sources* **230**, 230–235 (2013).
34. C. Masarapu, H. F. Zeng, K. H. Hung, B. Wei, Effect of temperature on the capacitance of carbon nanotube supercapacitors. *ACS Nano* **3**, 2199–2206 (2009).
35. B.-A. Mei, O. Munteshari, J. Lau, B. Dunn, L. Pilon, Physical interpretations of nyquist plots for EDLC electrodes and devices. *J. Phys. Chem. C* **122**, 194–206 (2017).
36. D. Kim, G. Lee, D. Kim, J. S. Ha, Air-stable, high-performance, flexible microsupercapacitor with patterned ionogel electrolyte. *ACS Appl. Mater. Interfaces* **7**, 4608–4615 (2015).
37. J. Li, S. Sollami Delekta, P. Zhang, S. Yang, M. R. Lohe, X. Zhuang, X. Feng, M. Ostling, Scalable fabrication and integration of graphene microsupercapacitors through full inkjet printing. *ACS Nano* **11**, 8249–8256 (2017).
38. T. Gao, Z. Zhou, J. Yu, J. Zhao, G. Wang, D. Cao, B. Ding, Y. Li, 3D printing of tunable energy storage devices with both high areal and volumetric energy densities. *Adv. Energy Mater.* **9**, 1802578 (2019).
39. X. Tang, H. Zhou, Z. Cai, D. Cheng, P. He, P. Xie, D. Zhang, T. Fan, Generalized 3D printing of graphene-based mixed-dimensional hybrid aerogels. *ACS Nano* **12**, 3502–3511 (2018).

40. X. Shi, S. Pei, F. Zhou, W. Ren, H.-M. Cheng, Z.-S. Wu, X. Bao, Ultrahigh-voltage integrated micro-supercapacitors with designable shapes and superior flexibility. *Energ. Environ. Sci.* **12**, 1534–1541 (2019).

Acknowledgments

Funding: This work was supported by the U.S. Army Research Office (ARO) (W911NF-18-1-0016), the Basic Science Research Program (2017M1A2A2087810 and 2018R1A2A1A05019733), Wearable Platform Materials Technology Center (2016R1A5A1009926) through the National Research Foundation of Korea (NRF) grant by the Korean Government (MSIT), Industry Technology Development Program (10080540) funded by the Ministry of Trade, Industry and Energy (MOTIE, Korea), National Institute of Forest Science (FP 0400-2016-01), and Batteries R&D of LG Chem. **Author contributions:** K.-H.L. designed the study, performed most of experiments, and analyzed all data analysis. S.-S.L. and D.B.A. participated in the characterization of electrochemical performances. J.L. and D.B. participated in discussing the EHD printing processes. S.-Y.L. coordinated and supervised the overall project. K.H.L. and S.-Y.L. wrote the manuscript, and all authors discussed the result and commented on the manuscript. **Competing interests:** The authors declare that they have no competing interests. **Data and materials availability**: All data needed to evaluate the conclusions in the paper are present in the paper and/or the Supplementary Materials. Additional data related to this paper may be requested from the authors.

Submitted 19 August 2019
Accepted 12 December 2019
Published 6 March 2020
10.1126/sciadv.aaz1692

Citation: K.-H. Lee, S.-S. Lee, D. B. Ahn, J. Lee, D. Byun, S.-Y. Lee, Ultrahigh areal number density solid-state on-chip microsupercapacitors via electrohydrodynamic jet printing. *Sci. Adv.* **6**, eaaz1692 (2020).

Science Advances

Ultrahigh areal number density solid-state on-chip microsupercapacitors via electrohydrodynamic jet printing

Kwon-Hyung Lee, Seong-Sun Lee, David B. Ahn, Jaehyun Lee, Doyoung Byun and Sang-Young Lee

Sci Adv **6** (10), eaaz1692.
DOI: 10.1126/sciadv.aaz1692

Science Advances (ISSN 2375-2548) is published by the American Association for the Advancement of Science, 1200 New York Avenue NW, Washington, DC 20005. The title *Science Advances* is a registered trademark of AAAS.